Accumulation of Lipid Droplets in a Novel Bietti Crystalline Dystrophy Zebrafish Model With Impaired PPARα Pathway

Pan Gao,[1] Danna Jia,[1] Pei Li,[1] Yuwen Huang,[1] Hualei Hu,[1] Kui Sun,[1] Yuexia Lv,[1] Xiang Chen,[1] Yunqiao Han,[1] Zuxiao Zhang,[1] Xiang Ren,[1] Qing Wang,[1] Fei Liu,[2,3] Zhaohui Tang,[1] and Mugen Liu[1]

[1]Key Laboratory of Molecular Biophysics of Ministry of Education, College of Life Science and Technology, Huazhong University of Science and Technology, Wuhan, Hubei, PR China
[2]State Key Laboratory of Freshwater Ecology and Biotechnology, Institute of Hydrobiology, The Innovative Academy of Seed Design, Hubei Hongshan Laboratory, Chinese Academy of Sciences, Wuhan, China
[3]University of Chinese Academy of Sciences, Beijing, China

Correspondence: Mugen Liu, Key Laboratory of Molecular Biophysics of Ministry of Education, College of Life Science and Technology, 1037, Luoyu Road, Wuhan, P. R. China; lium@hust.edu.cn.
Zhaohui Tang, Key Laboratory of Molecular Biophysics of Ministry of Education, College of Life Science and Technology, 1037, Luoyu Road, Wuhan, P. R. China; zh_tang@mail.hust.edu.cn.
Fei Liu, State Key Laboratory of Freshwater Ecology and Biotechnology, Institute of Hydrobiology, The Innovative Academy of Seed Design, Hubei Hongshan Laboratory, Chinese Academy of Sciences, Wuhan, China; liufei2018@ihb.ac.cn.

PG, DJ, and PL contributed equally to this work.

PURPOSE. Bietti crystalline dystrophy (BCD) is a progressive retinal degenerative disease primarily characterized by numerous crystal-like deposits and degeneration of retinal pigment epithelium (RPE) and photoreceptor cells. *CYP4V2* (cytochrome P450 family 4 subfamily V member 2) is currently the only disease-causing gene for BCD. We aimed to generate a zebrafish model to explore the functional role of *CYP4V2* in the development of BCD and identify potential therapeutic targets for future studies.

METHODS. The *cyp4v7* and *cyp4v8* (homologous genes of *CYP4V2*) knockout zebrafish lines were generated by CRISPR/Cas9 technology. The morphology of photoreceptor and RPE cells and the accumulation of lipid droplets in RPE cells were investigated at a series of different developmental stages through histological analysis, immunofluorescence, and lipid staining. Transcriptome analysis was performed to investigate the changes in gene expression of RPE cells during the progression of BCD.

RESULTS. Progressive retinal degeneration including RPE atrophy and photoreceptor loss was observed in the mutant zebrafish as early as seven months after fertilization. We also observed the excessive accumulation of lipid droplets in RPE cells from three months after fertilization, which preceded the retinal degeneration by several months. Transcriptome analysis suggested that multiple metabolism pathways, especially the lipid metabolism pathways, were significantly changed in RPE cells. The down-regulation of the peroxisome proliferator-activated receptor α (PPARα) pathway was further confirmed in the mutant zebrafish and *CYP4V2*-knockdown human RPE-1 cells.

CONCLUSIONS. Our work established an animal model that recapitulates the symptoms of BCD patients and revealed that abnormal lipid metabolism in RPE cells, probably caused by dysregulation of the PPARα pathway, might be the main and direct consequence of CYP4V2 deficiency. These findings will deepen our understanding of the pathogenesis of BCD and provide potential therapeutic approaches.

Keywords: CYP4V2, Bietti crystalline dystrophy, retinal degeneration, lipid droplets, PPARα

Bietti crystalline dystrophy (BCD) is an inherited progressive retinal degeneration disease that was first described in 1937 by Bietti.[1] BCD appears to be more common in East Asia, especially in Chinese and Japanese people.[2–6] The frequency of pathogenic alleles of BCD has been estimated to be 1:67000.[7,8] BCD patients often show clinical symptoms similar to those of retinitis pigmentosa (RP), including night blindness, progressive loss of visual field, vision decline, and eventually total blindness.[8] The numerous small crystal-like deposits in the fundus are the most obvious feature of BCD patients. Optical coherence tomography imaging studies of BCD patients showed that the crystals were predominantly located in the retinal pigment epithelium (RPE) layer.[9–12] The above clinical findings indicate that RPE may be the cell type that is predominantly damaged in BCD. Currently, there is no effective treatment for BCD.

Until now, mutations of *CYP4V2* (cytochrome P450 family 4 subfamily V member 2) are the only known genetic cause of BCD. Three mutations of *CYP4V2*, including c.802_810del17insGC, c.992A>C, and c.1091-2A>G,

account for more than 80% of the mutant alleles identified in BCD.[6,13–15] CYP4V2 is a member of the cytochrome P450 (CYP) 4 family of enzymes, which catalyzed the ω-hydroxylation of fatty acid.[16,17] In vitro experiments have shown that recombinant CYP4V2 can selectively hydroxylate long-chain and medium-long chain saturated and unsaturated fatty acids in the presence of NADPH.[18] Lai et al.[19] have reported a higher concentration of octadecanoic acid [18:0] and the lower concentrations of octadecadienoic acid [18:1n-9] and overall monounsaturated fatty acid in serum samples of 16 Chinese BCD patients. In the *Cyp4v3* knockout mouse model, changes in serum fatty acid composition were also observed, but in the opposite direction.[20]

More importantly, the exclusive ocular phenotypes found in BCD patients and the BCD mouse models suggest that the *CYP4V2* gene may play an essential role in these types of cells, especially the RPE cells. Recently, Hata et al.[21] have successfully generated BCD patient–specific RPE cells by induced pluripotent stem cell (iPSC) technology and revealed the accumulation of free cholesterol and the impairment of autophagy flux in these BCD-affected RPE cells. However, because of the difficulties in accessing RPE cells from BCD patients or appropriate animal models of BCD, their findings have not been verified in vivo. Therefore it is particularly important to establish appropriate animal models that could recapitulate the lipid metabolism defects and retinal degeneration phenotypes and so facilitate the molecular mechanism studies of BCD.

In the present study, we generated a BCD animal model by knocking out the homologous genes of *CYP4V2* in zebrafish through CRISPR/Cas9 technology. The accumulation of lipid droplets in RPE cells and the progressive degeneration of RPE and photoreceptor cells were observed. Furthermore, we performed transcriptome analysis on the isolated RPE cells to investigate the potential pathways mediated by *CYP4V2* and to identify the molecular mechanism underlying the abnormal lipid metabolism and the onset and progression of BCD.

MATERIALS AND METHODS

Zebrafish Husbandry

Zebrafish were cultured in a circulated water system at 28.5°C and in a daily cycle of 14-hour-light and 10-hour-dark. The study was approved by the Ethics Committee of Huazhong University of Science and Technology.

Mutants Generation by CRISPR/Cas9 Technology

The sgRNAs and Cas9 mRNA were synthesized using the Transcript Aid T7 High Yield Transcription Kit (K0441; Thermo Fisher Scientific, Waltham, MA, USA) and mMESSAGE mMACHINE T3 Transcription Kit (AM1348; Invitrogen, Carlsbad, CA, USA), respectively. Cas9 mRNA (300 ng/µL) and two sgRNAs for *cyp4v7* and *cyp4v8* genes (20 ng/µL each) were co-injected into the one-cell stage embryos.

Cryo-sectioning and Hematoxylin and Eosin (H&E) Staining

Whole zebrafish eyes were dissected and fixed in 4% paraformaldehyde. Then, the eyes were dehydrated in 30% sucrose and embedded in optical coherence tomography. Retinal sections with a thickness of 10 µm were cut with a cryostat (Leica CM1950; Leica, Wetzlar, Germany). Sections were stained with H&E for analysis. The sections after H&E staining were observed and photographed under the optical microscope BX53.

Nile Red Staining and Filipin Staining

Cryosections were used for Nile Red (cat. N-1142; Invitrogen) staining. The slides were washed with phosphate-buffered saline solution three times and incubated with Nile Red (2 µg/ml in DMSO) for 10 min in the dark. The nuclei were labeled with DAPI (5 µg/ml) for 5 min. The staining method for cultured cells is the same as above. RPE flat mounts were prepared as described and stained using the same protocol.[22] Filipin staining was performed using a cell-based cholesterol detection kit (Sigma, SAE0087). The cryosections were balanced at room temperature for 20 min and washed three times with phosphate-buffered saline solution, followed by incubation for two hours with Filipin III. The nuclei were stained with PI for five minutes. The sections were mounted under glass coverslips. Fluorescence images were captured using a confocal laser-scanning microscope (FluoView FV1000 confocal microscope; Olympus Imaging, Tokyo, Japan). Triglyceride and free cholesterol concentrations were measured by commercial kits (Beijing Solarbio Science & Technology Co. Ltd, Beijing, China) according to the manufacturer's instructions.

Transmission Electron Microscopy (TEM)

TEM was performed according to a previous report.[23] Ultrathin sections of 100 nm thickness were prepared using an ultramicrotome and stained for TEM.

Immunofluorescence and Western Blotting

The preparation of RPE flat mounts and immunofluorescence analysis were performed as described previously.[22,24] Fluorescent images were captured using a confocal laser-scanning microscope (FluoView FV1000 confocal microscope; Olympus Imaging). Fresh cells and zebrafish eyes were isolated and lysed in RIPA buffer. Lysates were mixed with loading buffer and boiled for 10 minutes. Protein samples were separated by SDS-PAGE and transferred to nitrocellulose membranes. The membranes were blocked for one hour in 5% skim milk and incubated with primary antibodies overnight at 4°C. The membranes were then washed three times in TBST for five minutes each and incubated with either a goat anti-rabbit or a goat anti-mouse HRP-conjugated secondary antibody (1:20,000; Thermo Fisher Scientific) for two hours at room temperature. The protein bands were detected using a ChemiDoc XRS[+] system (Bio-Rad Life Science, Hercules, CA, USA) with the SuperSignal Sensitivity Substrate (Thermo Fisher Scientific), and quantified with the Quantity One software (Bio-Rad Life Science).

In Situ Hybridization

In situ hybridization for retinal sections was performed as previously described.[25] Probes were synthesized and labeled with the Digoxigenin using the MAXIscript SP6/T7 Transcription Kit (Invitrogen).

RNA Isolation and Quantitative PCR

Total RNA samples were extracted by Trizol reagents (Takara Biotechnology Co., Kyoto, Japan) according to the manufacturer's instruction. The first strand cDNAs was synthesized by MMLV reverse transcriptase (Invitrogen). Quantitative PCR (qPCR) was performed using AceQ qPCR SYBR Green Master Mix (Vazyme Biotech, Nanjing, China) on the StepOnePlus quantitative PCR System (Life Technologies, Carlsbad, CA, USA) according to the manufacturer's instructions. The relative gene expression was quantified using the StepOne software v2.3. Gene primers are listed in Supplementary Table S2.

Transcriptional Profiling

Eyeballs from 7-month-old wildtype (WT) and *cyp4v7/cyp4v8* DKO zebrafish were dissected, and the RPE layer was collected. Total RNA samples were extracted by Trizol Regent. RNA sequencing was performed on an Illumina HiSeq2000 platform (Gene Denovo Biotechnology, Co., Ltd., Guangzhou, China). The trimmed mean of M values was used to normalize raw counts of samples. Differently expressed genes were identified by the edgeR and DESeq2 using the following cut-off values: FC>2 and adjusted *P* value <0.05. Kyoto Encyclopedia of Genes and Genomes (KEGG) enrichment analysis was performed with DAVID.

Cell Culture and RNA Interference

Human RPE-1 cells (American Type Culture Collection, CRL-4000) were cultured in DMEM (Gibco 11330057; Thermo Fisher Scientific) supplemented with 10% FBS. Human *CYP4V2* small interfering RNA (siRNA) was synthesized and purified by RiboBio (Guangzhou RiboBio, Guangzhou, China). The target sequence of *CYP4V2* siRNA (si*CYP4V2*) was ACAGAGATCCGAGATACTT. The siRNA duplexes targeting nonspecific sequences were used as negative control (siNC). Cells were transfected with siNC or si*CYP4V2* by Lipofectamine 3000 (L3000015, Invitrogen) for 72 hours and then collected according to the requirements of subsequent experiments.

Statistical Analysis

All data were presented as mean with SEM. Data groups were compared by Student's *t* tests (Prism 6.0 software; GraphPad Software, Inc., La Jolla, CA, USA). Differences between groups were considered statistically significant if $P < 0.05$.

RESULTS

Generation of the *cyp4v7/cyp4v8* Double-Knockout Zebrafish

In zebrafish, two proteins encoded by the *cyp4v7* and *cyp4v8* genes both showed a high degree of homology to CYP4V2. About 65% of amino acid residues are identical and 60% of amino acid residues are positive between zebrafish Cyp4v7/Cyp4v8 and human CYP4V2 (Supplementary Fig. S1). In addition, we constructed a phylogenetic tree based on the amino acid sequences of all CYP4 (cytochrome P450 gene 4) family proteins in human and zebrafish genomes using the maximum likelihood with 500 bootstrap replicates from MEGA 7.0 (Molecular Evolutionary Genetics Analysis).[26] As shown in Figure 1A, there are only four CYP4 family genes in zebrafish, and the *cyp4v7* and *cyp4v8* genes show the closest evolutionary distance to the human *CYP4V2* gene.

Next, we detected the expression distribution of *cyp4v7* and *cyp4v8* in zebrafish retinas by in situ hybridization (Fig. 1B). Noticeably, *cyp4v7* and *cyp4v8* were both widely expressed throughout the retina, and *cyp4v7* showed a relatively enriched expression in RPE cells. These expression patterns are similar to that of *CYP4V2* in human retinas reported previously.[18] The expression levels of *cyp4v7* and *cyp4v8* were also detected by semiquantitative reverse-transcription PCR. The mRNA level of *cyp4v7* was much higher than *cyp4v8* in zebrafish retinas (Fig. 1C). These results suggested that compared with other members in the CYP4 family of zebrafish, *cyp4v7* and *cyp4v8* are the most likely homologous genes of human *CYP4V2* in zebrafish.

To further confirm the functional conservation between zebrafish Cyp4v7/Cyp4v8 and human CYP4V2 and establish an appropriate BCD disease model, we generated the *cyp4v7* and *cyp4v8* double knockout (DKO) zebrafish line by CRISPR/Cas9 technology. Two sgRNA target sites in the exon 9 of *cyp4v7* and the exon 6 of *cyp4v8* (Fig. 1D), which are located in the corresponding mutational hotspots of human *CYP4V2*, were chosen for knockout experiments.[27] Through three rounds of screening, we obtained the *cyp4v7/cyp4v8* double knockout (named *cyp4v7/cyp4v8* DKO) zebrafish line (Fig. 1E). The mRNA levels of *cyp4v7* were reduced by about 50% in the mutant group compared with the WT group, although there was no significant decrease of *cyp4v8* mRNA levels (Fig. 1F). Meanwhile, we amplified and sequenced the cDNA fragments spanning the two mutations in *cyp4v7* and *cyp4v8*, respectively (Supplementary Fig. S2). There were no alternative splicing events that could skip the mutant exons, and the mutations indeed existed in the mature mRNAs of *cyp4v7* and *cyp4v8*. These results suggested that the functions of *cyp4v7* and *cyp4v8* are likely destroyed in the *cyp4v7/cyp4v8* DKO zebrafish.

Progressive Degeneration of Photoreceptor and RPE Cells in *cyp4v7/cyp4v8* DKO Zebrafish

To investigate the retinal phenotypes of the *cyp4v7/cyp4v8* DKO zebrafish, histological analysis was performed at 7, 10, 12, and 20 months after fertilization (Figs. 2A, 2B). At 7 and 10 mpf, there were no significant differences in the retinal structure or the thickness of retinal layers between WT and mutant zebrafish. However, at 12 mpf, we observed obvious attenuation of the photoreceptor layer, especially the outer segment layer, in *cyp4v7/cyp4v8* DKO zebrafish. This situation became much more severe at 20 mpf. The expression of rod-specific (Gnat1) and cone-specific (Gnat2) phototransduction cascade proteins were detected by Western blotting at 10 and 12 mpf (Fig. 2C). The protein levels of Gnat1 were decreased mildly at 10 mpf and severely at 12 mpf. Meanwhile, the protein levels of Gnat2 were unchanged at 10 mpf, but significantly decreased at 12 mpf (Figs. 2C, 2D). These results further supported the existence of progressive photoreceptor degeneration with a rod-first and cone-later pattern.

RPE cells are considered the main affected cells in BCD patients. Consequently, we checked the morphology of RPE cells in WT and *cyp4v7/cyp4v8* DKO zebrafish by immunostaining using the anti-ZO-1 antibody on RPE flat
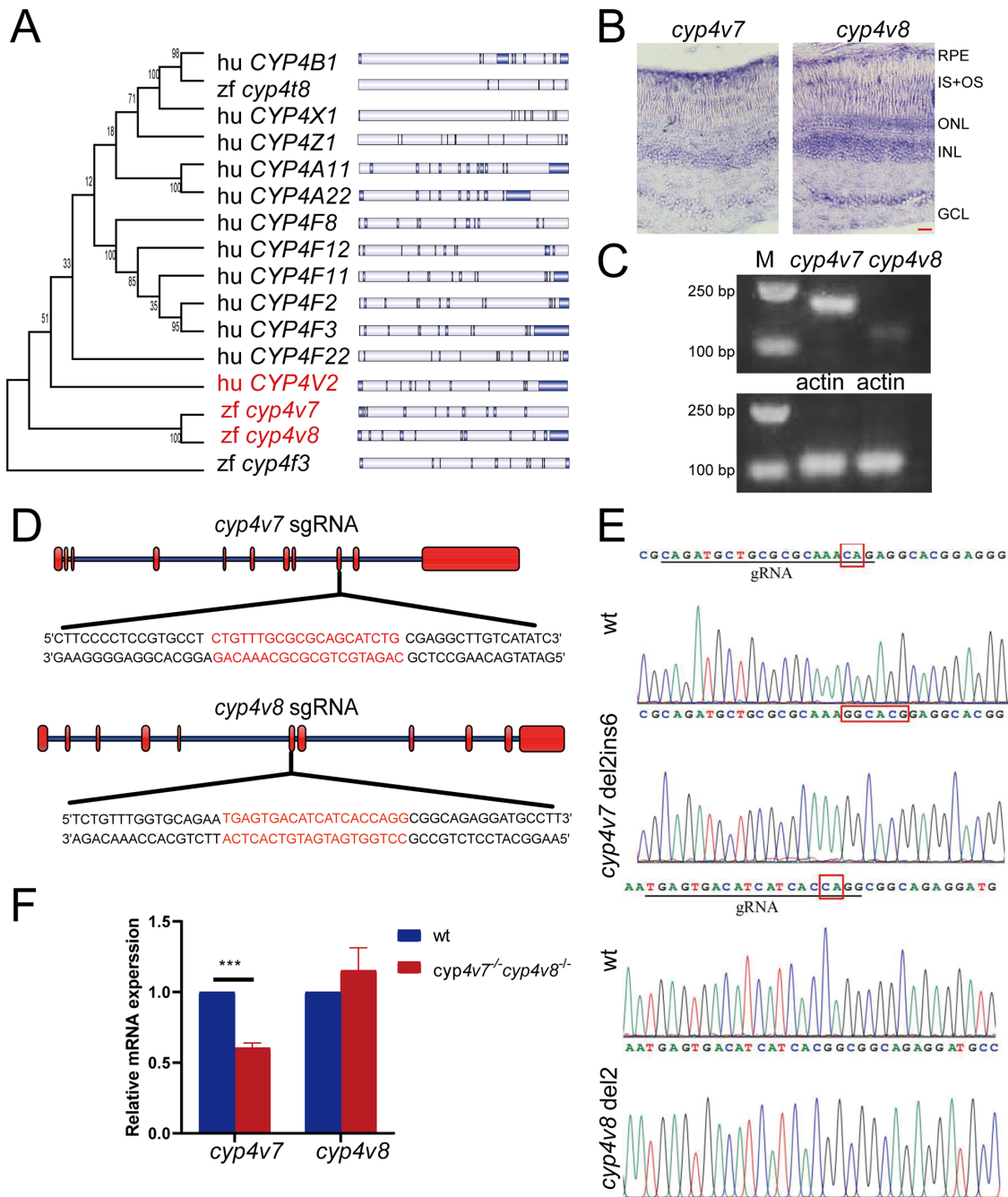
FIGURE 1. Generation of the *cyp4v7* and *cyp4v8* double knockout zebrafish. (**A**) Phylogenetic relationships and gene structures of CYP4 family genes in human and zebrafish. (**B**) In situ hybridization of *cyp4v7* and *cyp4v8* in retinas of two-month-old WT zebrafish. IS+OS, inner segment and outer segment; ONL, outer nuclear layer; INL, inner nuclear layer; GCL, ganglion cell layer. *Scale bars*: 20 μm. (**C**) Semiquantitative RT-PCR analysis of *cyp4v7* and *cyp4v8* expression in two-month-old zebrafish eyes. (**D**) CRISPR/Cas9 target sites. (**E**) DNA sequencing of the corresponding genomic region for WT and mutant zebrafish. The sequencing traces revealed a 2 bp deletion/6 bp insertion mutation in *cyp4v7* and a 2 bp deletion mutation in *cyp4v8*. (**F**) Relative mRNA levels of *cyp4v7* and *cyp4v8* were detected by qPCR in WT and *cyp4v7* and *cyp4v8* double knockout zebrafish at 1 mpf. The results are shown as mean ± SD. ***$P < 0.001$.

mounts from 7 to 20 months after fertilization (Fig. 3A). In *cyp4v7/cyp4v8* DKO zebrafish, the loss of hexagonal cellular architecture and junctional integrity RPE cells could be observed as early as seven after fertilization, suggesting the dysfunction and atrophy of RPE cells. The number of degenerative RPE cells increased with age dramatically in the mutant zebrafish (Fig. 3B). These results demonstrated that there was also progressive degeneration of RPE cells occurring before photoreceptor degeneration in the *cyp4v7/cyp4v8* DKO zebrafish.

Excessive Accumulation of Lipid Droplets in RPE Cells of *cyp4v7/cyp4v8* DKO Zebrafish

CYP4V2 is supposed to play a role in lipid metabolism.[28] We wondered whether there was abnormal lipid accumulation in the retina of *cyp4v7/cyp4v8* DKO zebrafish. We found that accumulation of lipid droplets (LDs) could be observed in RPE layer by Nile red staining in the *cyp4v7/cyp4v8* DKO zebrafish as early as 3 mpf (Fig. 4A). RPE flat mounts of WT and *cyp4v7/cyp4v8* DKO zebrafish were also prepared
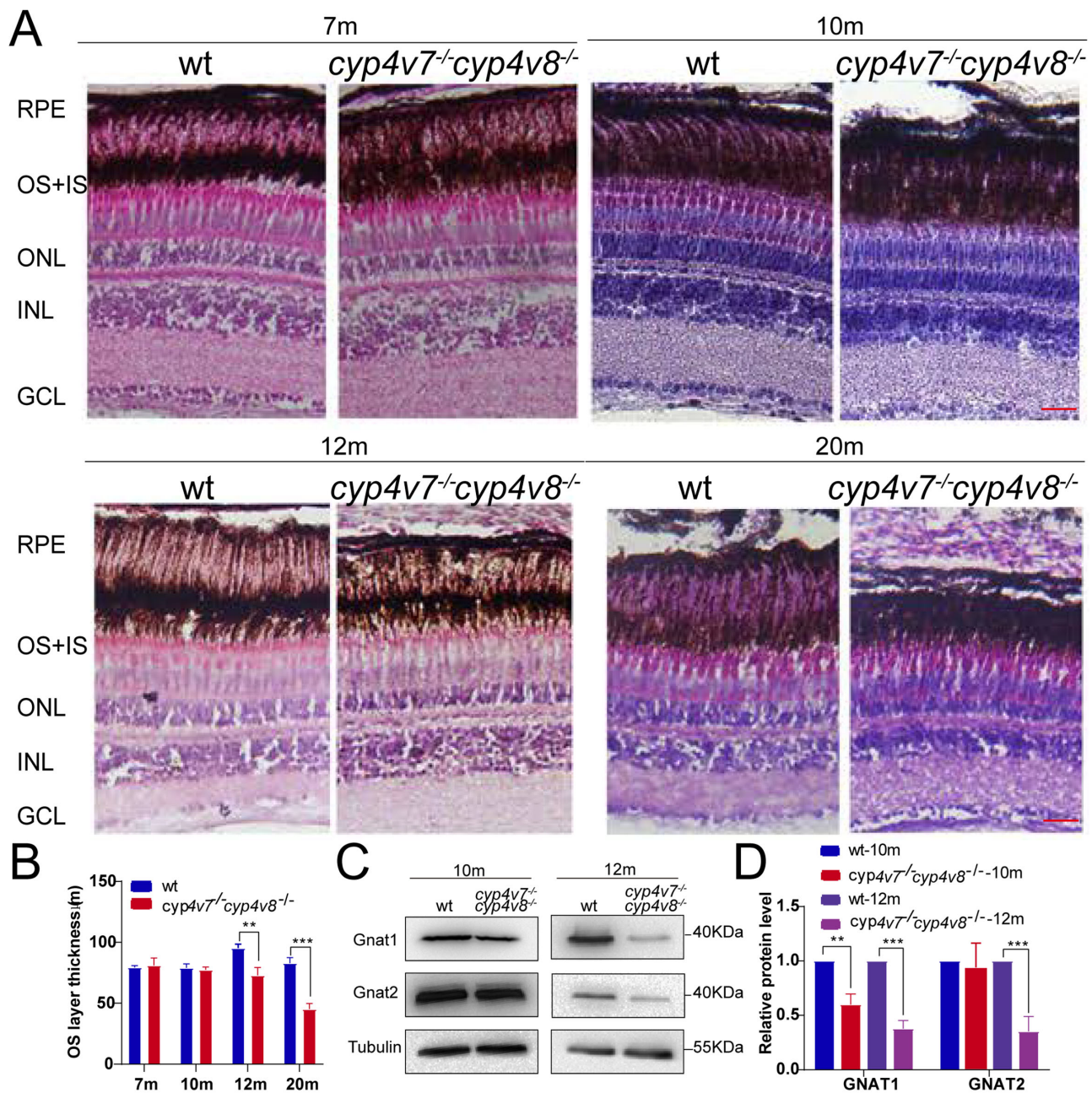
FIGURE 2. Progressive degeneration of photoreceptor cells in *cyp4v7/cyp4v8* DKO zebrafish. (**A**) Histological analysis revealed the progressive degeneration of the outer retinal layer in *cyp4v7*−/− *cyp4v8*−/− zebrafish. OS, outer segment; IS, inner segment; ONL, outer nuclear layer; INL, inner nuclear layer; GCL, ganglion cell layer. *Scale bars*: 20 μm. (**B**) The quantitative results of the thickness of OS layer (represented by the length from the lower edge of IS to the upper edge of RPE) in **A**. Three parallel samples were tested for each group. The results are shown as mean ± SD. ***$P < 0.001$; **$P < 0.01$. (**C**) Western blotting analysis of Gnat1 and Gnat2 protein levels in WT and mutant zebrafish retinas at 10 and 12 months after fertilization. Tubulin was used to normalize protein loading. (**D**) Quantitative analysis of the Western blot data. At least three independent experiments were performed and quantified. The results are shown as mean ± SD. ***$P < 0.001$; **$P < 0.01$.

and stained with Nile Red. LDs could be observed in nearly all RPE cells in the mutant zebrafish at 10 months after fertilization (Fig. 4B). From 3 to 10 months after fertilization, the number and size of LDs located in the RPE cells were significantly increased with age (Fig. 4B). The existence of LDs in RPE cells of *cyp4v7/cyp4v8* DKO zebrafish was further validated by TEM (Fig. 4C). These results suggested that the excessive accumulation of lipid droplets in RPE cells may be a major pathological change at the cellular

level before photoreceptor degeneration in the progression of BCD.

Accumulation of free cholesterol has been reported in the BCD iPSC-RPE cells.[21] We also detected the content of cholesterol in the retinas of WT and *cyp4v7/cyp4v8* DKO zebrafish by Filipin staining (Supplementary Fig. S3). No significant accumulation in free cholesterol was observed in 3-month-old *cyp4v7/cyp4v8* DKO zebrafish. However, at 12 months after fertilization, free cholesterol was specifically
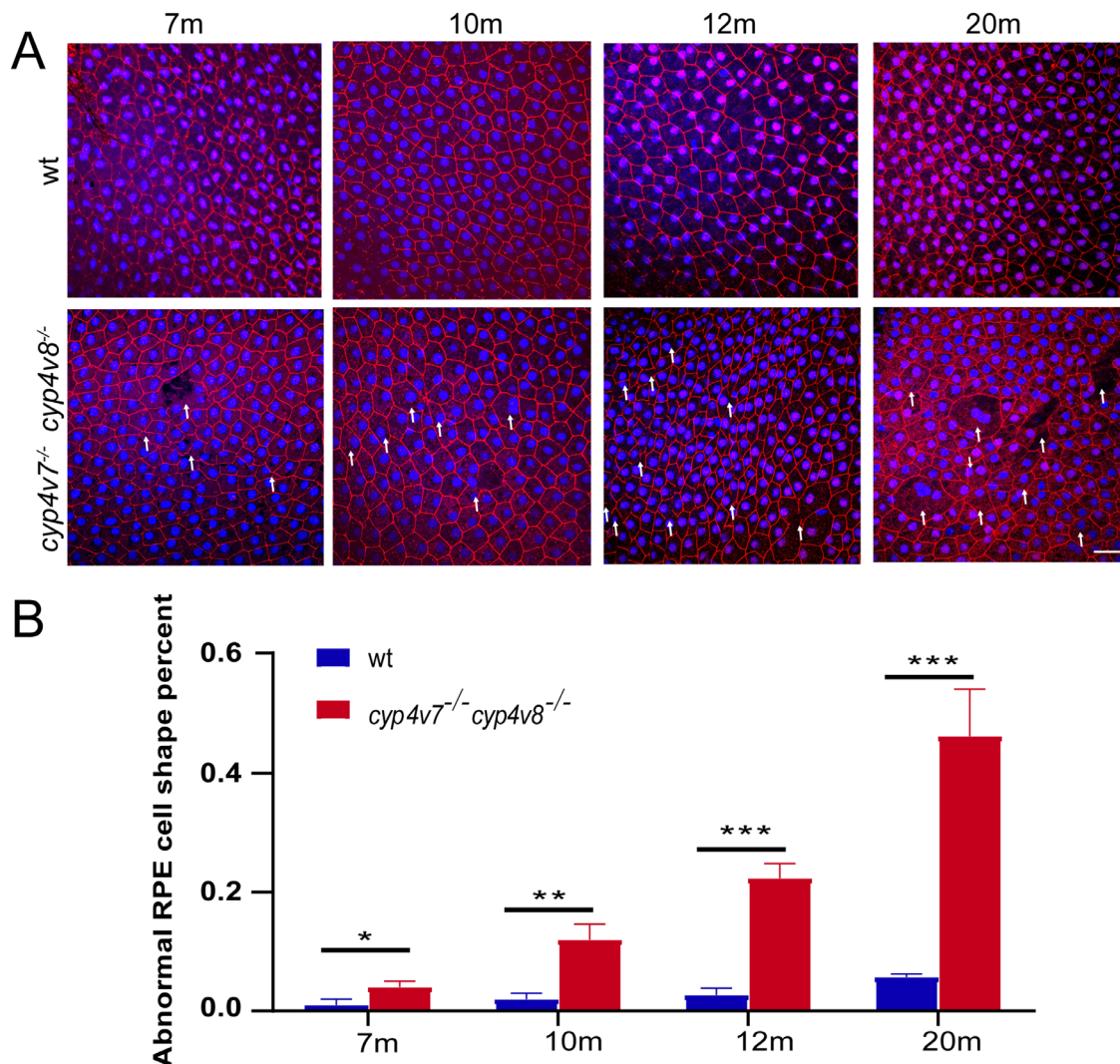
FIGURE 3. Abnormal morphologic characteristics of RPE cells in *cyp4v7/cyp4v8* DKO zebrafish. (**A**) Immunofluorescence analysis of flat-mounted eyecups from WT and *cyp4v7$^{-/-}$ cyp4v8$^{-/-}$* zebrafish at 7, 10, 12, and 20 months after fertilization using the anti-ZO-1 antibody. We defined the loss of hexagonal cellular architecture and junctional integrity cells as abnormal RPE cells. *White arrows* indicate the abnormal RPE cells. *Scale bar*: 20 μm. (**B**) The numbers of abnormal RPE cells were quantified for each of the images. The results are shown as mean ± SD. ***$P < 0.001$; **$P < 0.01$; *$P < 0.05$.

enriched in the RPE layer of *cyp4v7/cyp4v8* DKO retinas, compared with WT retinas. Our result suggested that free cholesterol accumulation might be a feature of BCD in the middle and late stages and is likely not the direct cause of CYP4V2 deficiency.

Downregulation of the PPARα Pathway is Involved in the Accumulation of Lipids Caused by CYP4V2 Deficiency

To investigate the molecular mechanism underlying the onset and development of BCD, we performed transcriptional profiling of the RPE tissues from WT and *cyp4v7/cyp4v8* DKO zebrafish at seven months after fertilization by RNA sequencing (RNA-seq). A total of 3170 differentially expressed genes were identified, of which 1341 were upregulated and 1829 were downregulated (Fig. 5A). The top 20 KEGG enriched pathways (Fig. 5B) involved in

metabolism processes accounted for 30% of all pathways. The lipid metabolism pathways could be further divided into bile acid biosynthesis, arachidonic acid metabolism, steroid biosynthesis, linoleic acid metabolism, and fatty acid elongation (Fig. 5C). Interestingly, some of the lipid metabolism-related genes were regulated by peroxisome proliferators activated receptors alpha (PPARα), and its pathway (ko03320) also significantly enriched in the top 20 KEGG pathways. Furthermore, we checked the expression of genes involved in the PPARα pathway by showing them in the heatmap based on our RNA-seq data (Fig. 5D). The fabp (fatty acid binding protein) family genes (*fabp1a, fabp7a, fabp7b, fabp11a, fabp11b*) and other PPARα-regulated genes such as apo-AI (apolipoprotein A-I) and *cyp27a1.2* (cytochrome P450 family 7 subfamily A member 27a) were significantly downregulated, which was also verified by qPCR (Fig. 5E). We also observed the decreased protein levels of PPARα in 7-month-old *cyp4v7/cyp4v8* DKO zebrafish (Fig. 5F). Finally, we knocked
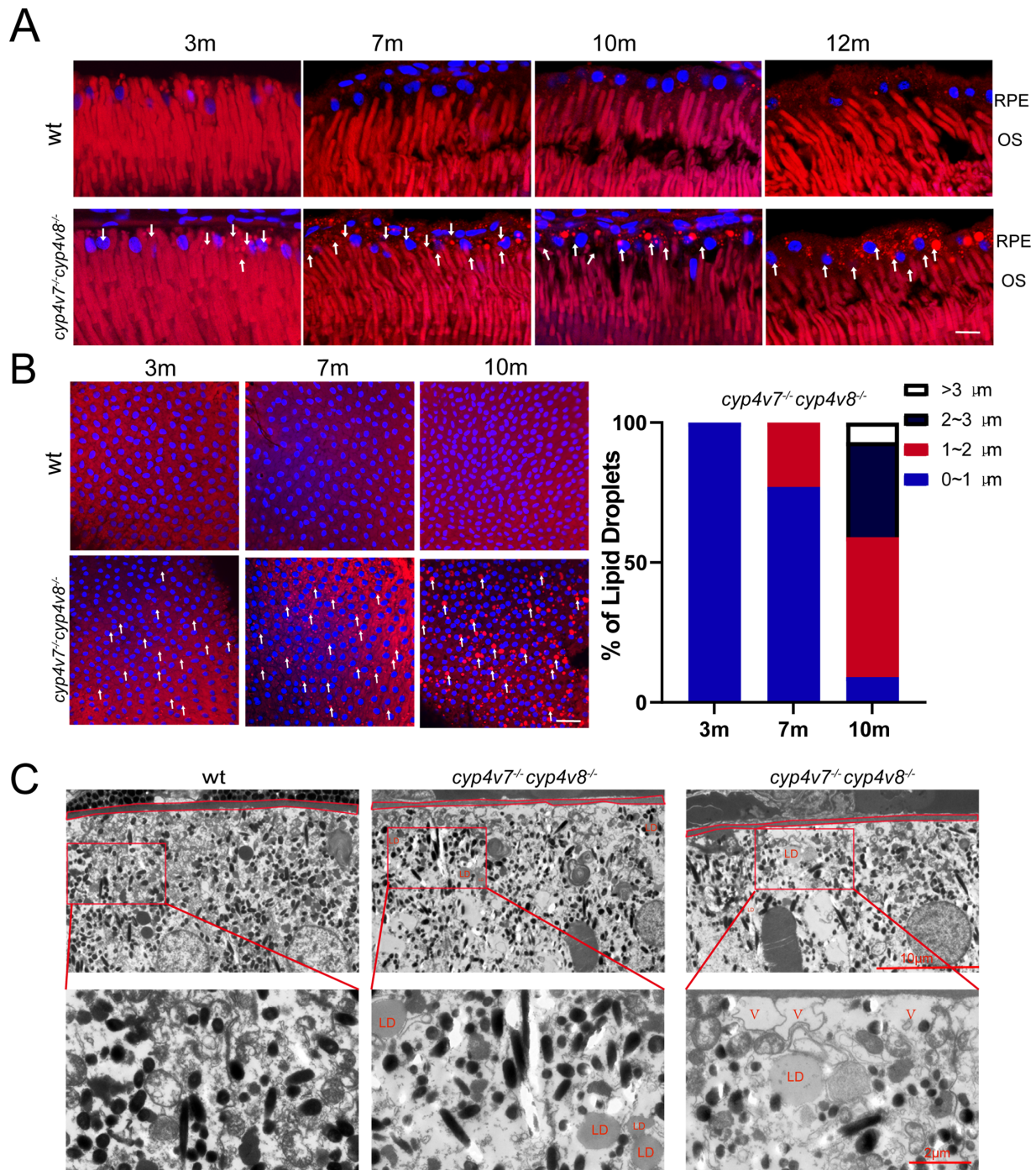
FIGURE 4. Lipid accumulation in RPE cells of WT and $cyp4v7^{-/-}$ $cyp4v8^{-/-}$ zebrafish. (**A**) Nile red staining of lipid droplets in retinal frozen sections of WT and $cyp4v7^{-/-}$ $cyp4v8^{-/-}$ zebrafish at 3, 7, 10, and 12 mpf. *White arrows*, lipid droplets. *Scale bar*: 20 µm. (**B**) Nile red staining of RPE flat mounts from WT and $cyp4v7^{-/-}$ $cyp4v8^{-/-}$ zebrafish at 3, 7, and 10 months after fertilization. *White arrows*, lipid droplets (*bright red*). *Scale bar*: 20 µm. *Bar graphs* show LD size distribution in $cyp4v7^{-/-}$ $cyp4v8^{-/-}$ zebrafish RPE flat mounts at 3, 7, and 10 months after fertilization. Diameter of LDs in $cyp4v7^{-/-}$ $cyp4v8^{-/-}$ zebrafish RPE cell was measured and represented by *white* (>3 µm), *black* (2-3 µm), *red* (1-2 µm), and *blue* (0-1 µm) (n = 88-103 RPE cells examined over three biologically independent experiments). (**C**) TEM images of retinal ultrathin sections from WT and $cyp4v7^{-/-}$ $cyp4v8^{-/-}$ zebrafish at seven months after fertilization. Lipid droplets are labeled with *red text "LD"*. Vacuoles are labeled with red text "V."

down the expression of CYP4V2 in the human RPE-1 cell line by siRNA interference and detected the change of PPARα protein levels. Similar to what we found in the BCD zebrafish model, knockdown of CYP4V2 alleviate the PPARα protein level (Fig. 6A). Moreover, the accumulation of LDs and

increased levels of triglycerides and free cholesterol were also observed in CYP4V2-depleted human RPE-1 cells (Figs. 6B–E). These results suggested a conserved and probably direct role of CYP4V2 in the regulation of PPARα pathway and lipid metabolism.
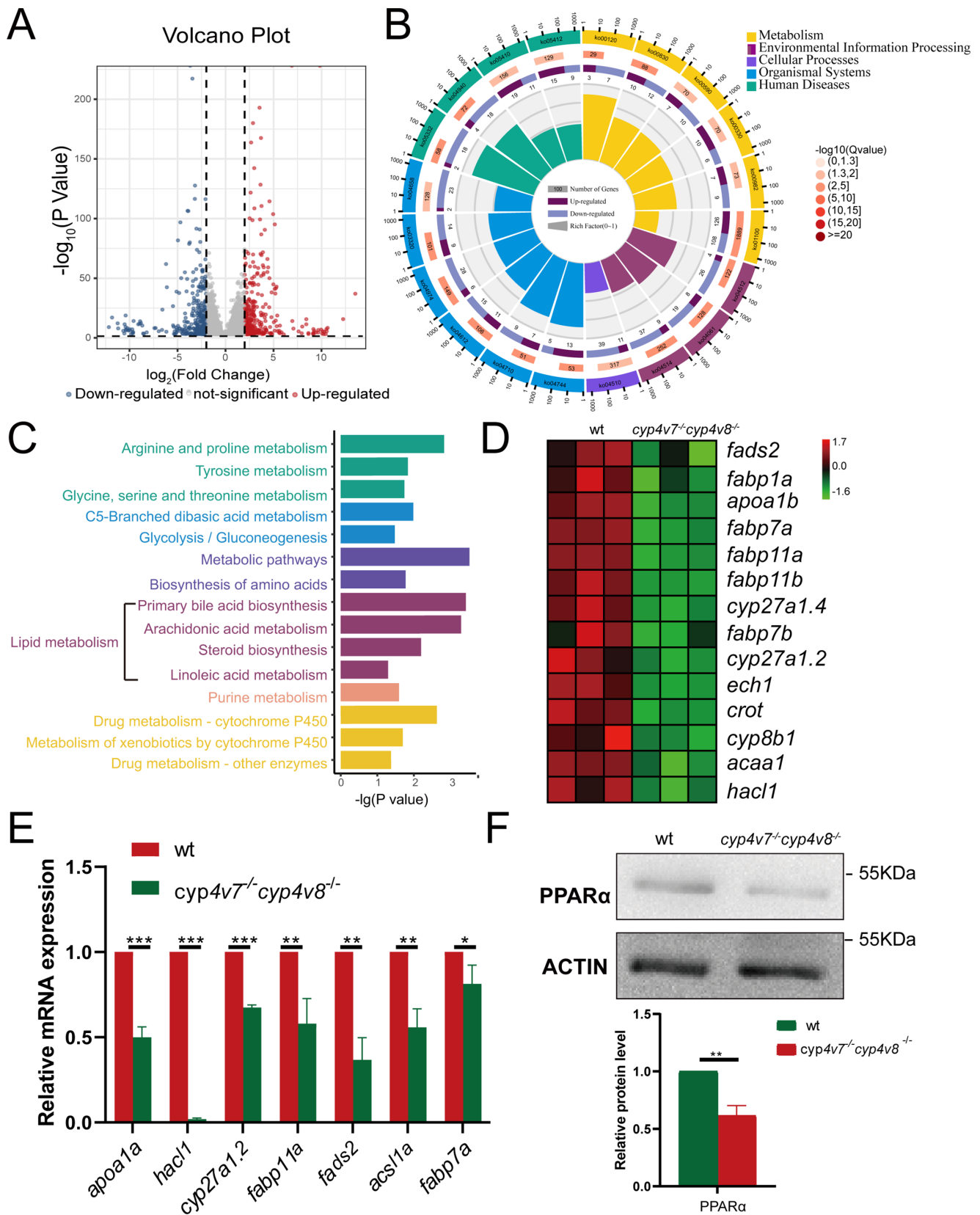
FIGURE 5. Downregulation of the PPARα pathway was involved in *cyp4v7*/*cyp4v8* DKO zebrafish RPE cells. (**A**) Volcano plot of differentially expressed genes in *cyp4v7*$^{-/-}$ *cyp4v8*$^{-/-}$ zebrafish compared with WT. (**B**) KEGG circle enrichment analysis of the differentially expressed genes. The first lap indicates the top 20 KEGG terms. The second lap represents the gene numbers in the genome backdrop. The third circle represents the ratio of the upregulated genes (*dark purple*) and downregulated genes (*light purple*). The fourth circle represents the enrichment element of each KEGG term. (**C**) KEGG enriched metabolism pathways (*P* < 0.05) are shown. (**D**) Expression patterns of genes in PPARα signaling pathway in WT and *cyp4v7*$^{-/-}$ *cyp4v8*$^{-/-}$ zebrafish RPE cells are shown in the heatmap. (**E**) Validation of the expression

of genes in PPARα pathway by qPCR in *cyp4v7* and *cyp4v8* DKO zebrafish RPE cells at seven months after fertilization. (**F**) Detection of the protein level of PPARα in WT and *cyp4v7$^{-/-}$ cyp4v8$^{-/-}$* zebrafish RPE cells by Western blot. The results are shown as mean ± SD. ***P < 0.001; **P < 0.01; *P < 0.05.
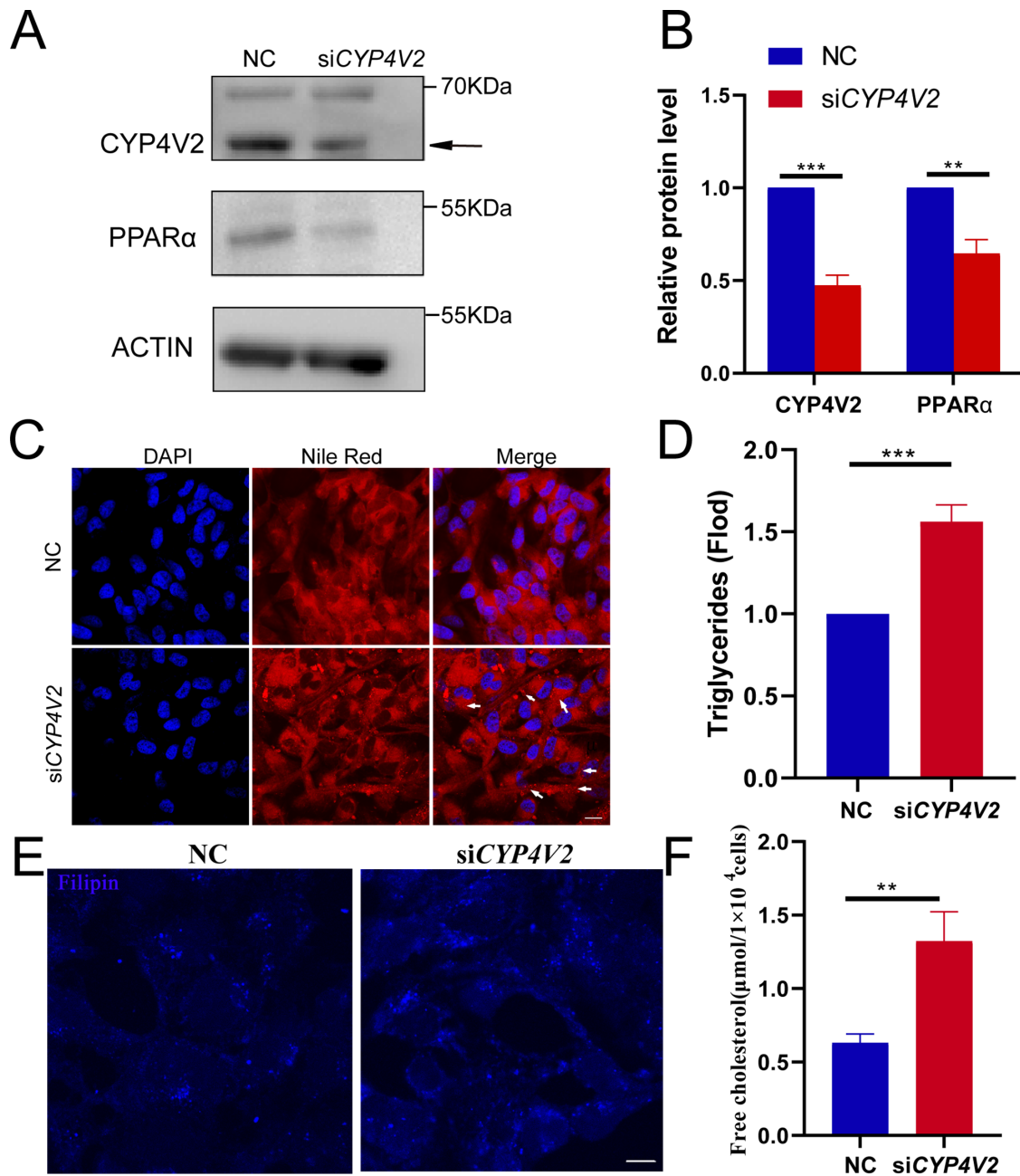

FIGURE 6. Knockdown of *CYP4V2* increases LDs and free cholesterol accumulation in human RPE-1 cells. (**A**) Analysis of CYP4V2 and PPARα protein levels in negative control (NC) and si*CYP4V2* RPE-1 cells by Western blotting. (**B**) Quantitative analysis of the Western blot data. At least three independent experiments were performed and quantified. The results are shown as mean ± SD. **P < 0.01. (**C**) Increased LDs in si*CYP4V2* RPE-1 cells as revealed by Nile red staining. *Scale bar*: 10 µm. (**D**) Measurement of triglyceride concentrations in NC and si*CYP4V2* RPE-1 cells. (**E**) Filipin staining in NC and si*CYP4V2* RPE-1 cells. *Scale bar*, 10 µm. (**F**) Free cholesterol concentration in NC and si*CYP4V2* RPE-1 cells. The results are shown as mean ± SD. ***P < 0.001; **P < 0.01.

DISCUSSION

In this study, we generated a novel BCD animal model by knocking out the homologous genes of *CYP4V2* in zebrafish.

The progressive degeneration of RPE and photoreceptor cells and the accumulation of lipid droplets in RPE cells suggest that the *cyp4v7/cyp4v8* double knockout zebrafish is an appropriate model for BCD, in addition to the *cyp4v3-*

knockout mice reported in 2014.[20] Compared with the *CYP4V2* KO mice, we have made several important improvements in this study. First of all, we described a more detailed cellular phenotype during the progression of retinal degeneration in the *cyp4v7/cyp4v8* double knockout zebrafish. Our results clearly showed that RPE cells were affected first, which was followed by the rod and then cone photoreceptors. This degenerating pattern is highly consistent with the clinical findings from BCD patients. Second, we paid close attention to the changes in lipids in RPE cells. By a variety of means, we demonstrated that lipid droplets are mainly accumulated inside RPE cells but no other retinal cell types in an age-related manner. Third, we have tried to reveal the molecular mechanisms of BCD through transcriptome analysis using the RPE tissues isolated from WT and *cyp4v7/cyp4v8* double knockout zebrafish. We found that downregulation of the PPAR*α* pathway may be involved in the lipid accumulation caused by CYP4V2 deficiency in both zebrafish RPE cells and cultured human RPE cells. Furthermore, as a popular laboratory animal model, zebrafish demonstrated many advantages, such as the short growth cycle, the low breeding cost, the strong reproductive ability, the small body size, and the convenience for genetic manipulation and drug screening. Establishment of the BCD zebrafish model will provide sufficient experimental materials and lay a solid foundation for further studies in the related fields.

BCD has been considered as a lipid metabolic disorder for a long time. However, because of the limitation of material, this assumption has not been experimentally confirmed until recently. Two previous studies have analyzed serum lipid constituents in, respectively, BCD patients and the BCD mouse model, although inconsistent results were reported.[19,20] The major shortcoming is that the data obtained from serum samples may not accurately reflect the conditions in the mainly damaged tissues, such as the retina, in BCD. Besides, only a few types of lipids were tested in the two previous studies. In 2018, Hata et al.[21] performed untargeted lipidomics in BCD iPSC-RPE cells and found the accumulation of various glucosylceramides and free cholesterol. However, lipid analysis in another BCD iPSC-RPE model reported in 2020 revealed the accumulation of lipid droplets caused by poly-unsaturated fatty acid accumulation.[29] In our BCD zebrafish model, we also observed the accumulation of lipid droplets and free cholesterol in RPE cells in an age-related manner. However, there are still many differences among the three models in detail, probably because of the following reasons: (1) Lack of interactions between RPE cells and photoreceptors and choroid may cause unpredictable consequences in the in vitro cultured RPE cells; (2) Unlike what we have achieved with animal models, it is difficult to match the in vitro cultured RPE cells to the different stages of BCD progression. Therefore a time-course and comprehensive lipidomics analysis of RPE cells in the BCD zebrafish model helped to clarify the above questions and provided cues for further studies.

The mechanisms by which CYP4V2 deficiency causes abnormal lipid accumulation and retinal degeneration remain inconclusive. Dysfunctions of lysosomes and mitochondria have been reported in the two BCD iPSC-RPE models, respectively.[21,29] In this study, we revealed that inhibition of the PPAR*α* pathway may be responsible for the lipid accumulation caused by CYP4V2 deficiency. It remains to be demonstrated whether the three mechanisms complement each other or function at different stages of BCD development. PPAR*α* is a ligand-inducible transcription factor controlling multiple processes in lipid metabolism, such as microsomal, peroxisomal, and mitochondrial fatty acid oxidation, synthesis, and breakdown of triglycerides, fatty acid binding and activation, fatty acid elongation, and desaturation.[30–35] A variety of endogenous fatty acids and their metabolites can bind to PPAR*α* as ligands and regulate lipid metabolism.[36] A reasonable assumption is that dysfunction of CYP4V2 may cause the reduction of certain bioactive metabolites that could activate the PPAR*α* pathway as ligands. This will also be investigated in our future studies.

In summary, we generated an interesting BCD zebrafish model and investigated the retinal phenotypes and pathogenic mechanisms by a combination of multiple technologies. The accumulation of lipid droplets in RPE cells was observed and became more substantial with increased age. Down-regulation of the PPAR*α* pathway was discovered in both RPE cells of BCD zebrafish and the *CYP4V2*-knockdown human RPE cell line, suggesting a conserved and causative role of CYP4V2 in regulating the PPAR*α* pathway. These findings will deepen our understanding of the pathogenesis of BCD and provide potential therapeutic targets for future studies.

Disclosure: **P. Gao,** None; **D. Jia,** None; **P. Li,** None; **Y. Huang,** None; **H. Hu,** None; **K. Sun,** None; **Y. Lv,** None; **X. Chen,** None; **Y. Han,** None; **Z. Zhang,** None; **X. Ren,** None; **Q. Wang,** None; **F. Liu,** None; **Z. Tang,** None; **M. Liu,** None

References

1. Bietti G. Ueber familiaeres Vorkommen Von "Retinitis punctata albescens" (Verbunden mit "Dystropllia marginalis cristallinea comeae"). *Klin Mbl AugeIllleilk.* 1937(99):739–757.
2. Lai TY, Ng TK, Tam PO, et al. Genotype phenotype analysis of Bietti's crystalline dystrophy in patients with CYP4V2 mutations. *Invest Ophthalmol Vis Sci.* 2007;48:5212–5220.
3. Gekka T, Hayashi T, Takeuchi T, et al. CYP4V2 mutations in two Japanese patients with Bietti's crystalline dystrophy. *Ophthalmic Res.* 2005;37:262–269.
4. Jin ZB, Ito S, Saito Y, et al. Clinical and molecular findings in three Japanese patients with crystalline retinopathy. *Jpn J Ophthalmol.* 2006;50:426–431.
5. Lin J, Nishiguchi KM, Nakamura M, et al. Recessive mutations in the CYP4V2 gene in East Asian and Middle Eastern patients with Bietti crystalline corneoretinal dystrophy. *J Med Genet.* 2005;42(6):e38.
6. Xiao X, Mai G, Li S, et al. Identification of CYP4V2 mutation in 21 families and overview of mutation spectrum in Bietti crystalline corneoretinal dystrophy. *Biochem Biophys Res Commun.* 2011;409:181–186.
7. Mataftsi A, Zografos L, Milla E, et al. Bietti's crystalline corneoretinal dystrophy: a cross-sectional study. *Retina.* 2004;24:416–426.
8. Miyata M, Ooto S, Ogino K, et al. Evaluation of photoreceptors in Bietti crystalline dystrophy with CYP4V2 mutations

using adaptive optics scanning laser ophthalmoscopy. *Am J Ophthalmol*. 2016;161:196–205.e191.

9. Halford S, Liew G, Mackay DS, et al. Detailed phenotypic and genotypic characterization of Bietti crystalline dystrophy. *Ophthalmology*. 2014;121:1174–1184.

10. Kojima H, Otani A, Ogino K, et al. Outer retinal circular structures in patients with Bietti crystalline retinopathy. *Br J Ophthalmol*. 2012;96:390–393.

11. Kaiser-Kupfer MI, Chan C-C, Markello TC, et al. Clinical biochemical and pathologic correlations in Bietti's crystalline dystrophy. *Am J Ophthalmol*. 1994;118:569–582.

12. Wilson DJ, Weleber RG, Klein ML, Welch RB, Green WR. Bietti's crystalline dystrophy. A clinicopathologic correlative study. *Ophthalmol*. 1989;107:213–221.

13. Meng XH, Guo H, Xu HW, et al. Identification of novel CYP4V2 gene mutations in 92 Chinese families with Bietti's crystalline corneoretinal dystrophy. *Mol Vis*. 2014;20:1806–1814.

14. Yin X, Yang L, Chen N, et al. Identification of CYP4V2 mutation in 36 Chinese families with Bietti crystalline corneoretinal dystrophy. *Exp Eye Res*. 2016;146:154–162.

15. Jarrar YB, Lee SJ. Molecular functionality of cytochrome P450 4 (CYP4) genetic polymorphisms and their clinical implications. *Int J Mol Sci*. 2019;20:4274.

16. Nakano M, Kelly EJ, Wiek C, et al. CYP4V2 in Bietti's crystalline dystrophy: ocular localization, metabolism of omega-3-polyunsaturated fatty acids, and functional deficit of the p.H331P variant. *Mol Pharmacol*. 2012;82:679–686.

17. Kelly EJ, Nakano M, Rohatgi P, et al. Finding homes for orphan cytochrome P450s: CYP4V2 and CYP4F22 in disease states. *Mol Interv*. 2011;11:124–132.

18. Nakano M, Kelly EJ, Rettie AE. Expression and characterization of CYP4V2 as a fatty acid omega-hydroxylase. *Drug Metab Dispos*. 2009;37:2119–2122.

19. Lai TY, Chu KO, Chan KP, et al. Alterations in serum fatty acid concentrations and desaturase activities in Bietti crystalline dystrophy unaffected by CYP4V2 genotypes. *Invest Ophthalmol Vis Sci*. 2010;51(2):1092–1097.

20. Lockhart CM, Nakano M, Rettie AE, et al. Generation and characterization of a murine model of Bietti crystalline dystrophy. *Invest Ophthalmol Vis Sci*. 2014;55:5572–5581.

21. Hata M, Ikeda HO, Iwai S, et al. Reduction of lipid accumulation rescues Bietti's crystalline dystrophy phenotypes. *Proc Natl Acad Sci USA*. 2018;115:3936–3941.

22. Storti F, Klee K, Todorova V, et al. Impaired ABCA1/ABCG1-mediated lipid efflux in the mouse retinal pigment epithelium (RPE) leads to retinal degeneration. *Elife*. 2019;8:e45100.

23. Qu Z, Yimer TA, Xie S, et al. Knocking out lca5 in zebrafish causes cone-rod dystrophy due to impaired outer segment protein trafficking. *Biochim Biophys Acta Mol Basis Dis*. 2019;1865:2694–2705.

24. Oczos J, Sutter I, Kloeckener-Gruissem B, et al. Lack of paraoxonase 1 alters phospholipid composition, but not morphology and function of the mouse retina. *Invest Ophthalmol Vis Sci*. 2014;55:4714–4727.

25. Brent AE, Schweitzer R, Tabin CJ. A somitic compartment of tendon progenitors. *Cell*. 2003;113:235–248.

26. Kumar S, Stecher G, Tamura K. MEGA7: Molecular Evolutionary Genetics Analysis Version 7.0 for Bigger Datasets. *Mol Biol Evol*. 2016;33:1870–1874.

27. Lee J, Jiao XD, Hejtmancik JF, et al. The metabolism of fatty acids in human Bietti crystalline dystrophy. *Invest Ophthalmol Vis Sci*. 2001;42:1707–1714.

28. Mackay DS, Halford S. Focus on molecules: cytochrome P450 family 4, subfamily V, polypeptide 2 (CYP4V2). *Exp Eye Res*. 2012;102:111–112.

29. Zhang Z, Yan B, Gao F, et al. PSCs Reveal PUFA-provoked mitochondrial stress as a central node potentiating RPE degeneration in Bietti's crystalline dystrophy. *Mol Ther*. 2020;28:2642–2661.

30. Islinger M, Cardoso MJ, Schrader M. Be different—the diversity of peroxisomes in the animal kingdom. *Biochim Biophys Acta*. 2010;1803:881–897.

31. Bougarne N, Weyers B, Desmet SJ, et al. Molecular actions of PPARalpha in lipid metabolism and inflammation. *Endocr Rev*. 2018;39:760–802.

32. Dubois V, Eeckhoute J, Lefebvre P, et al. Distinct but complementary contributions of PPAR isotypes to energy homeostasis. *J Clin Invest*. 2017;127:1202–1214.

33. Feige JN, Gelman L, Michalik L, et al. From molecular action to physiological outputs: peroxisome proliferator-activated receptors are nuclear receptors at the crossroads of key cellular functions. *Prog Lipid Res*. 2006;45:120–159.

34. Lefebvre P, Chinetti G, Fruchart JC, et al. Sorting out the roles of PPAR alpha in energy metabolism and vascular homeostasis. *J Clin Invest*. 2006;116:571–580.

35. Pyper SR, Viswakarma N, Yu S, et al. PPARalpha: energy combustion, hypolipidemia, inflammation and cancer. *Nucl Recept Signal*. 2010;8:e002.

36. Bishop-Bailey D, Wray J. Peroxisome proliferator-activated receptors: a critical review on endogenous pathways for ligand generation. *Prostaglandins Other Lipid Mediat*. 2003;71(1-2):1–22.